

PAPER

## Enhanced stability of plasmonic polymer solar cells using ferrocenedicarboxylic acid modification

To cite this article: Wujian Mao *et al* 2019 *Mater. Res. Express* **6** 075508

View the [article online](#) for updates and enhancements.



**IOP | ebooks™**

Bringing you innovative digital publishing with leading voices to create your essential collection of books in STEM research.

Start exploring the collection - download the first chapter of every title for free.

# Materials Research Express



## PAPER

# Enhanced stability of plasmonic polymer solar cells using ferrocenedicarboxylic acid modification

RECEIVED  
19 February 2019

REVISED  
12 March 2019

ACCEPTED FOR PUBLICATION  
29 March 2019

PUBLISHED  
10 April 2019

Wujian Mao<sup>1</sup>, Jiankai Zhang<sup>1</sup>, Jianping Zhou<sup>2</sup>, Sumei Huang<sup>1</sup> , Zhejuan Zhang<sup>1</sup>, Wei Ou-Yang<sup>1</sup> , Zhuo Sun<sup>1</sup> and Xiaohong Chen<sup>1</sup> 

<sup>1</sup> Engineering Research Center for Nanophotonics & Advanced Instrument, Ministry of Education, School of Physics and Materials Science, East China Normal University, Shanghai 200062, People's Republic of China

<sup>2</sup> School of Automation Engineering, Shanghai University of Electric Power, Shanghai 200090, People's Republic of China

E-mail: [xhchen@phy.ecnu.edu.cn](mailto:xhchen@phy.ecnu.edu.cn)

**Keywords:** polymer solar cells, UV stability, Ag nanoparticles, ferrocenedicarboxylic acid

## Abstract

The power conversion efficiency (PCE) of polymer solar cells (PSCs) can obviously be improved by plasmon resonance effects of noble metal nanoparticles. However, incorporating noble metal such as Ag and Au nanoparticles (NPs) can usually accelerate the deterioration of PSCs due to the diffusion of noble metal atoms, which would limit the potential application of plasmonic PSCs. PSCs with ferrocenedicarboxylic acid (FDA) modified Al-doped ZnO (AZO) layer compared to pure AZO layer can synchronously increase PCEs and ultraviolet (UV) and moisture stabilities. PSCs with Ag NPs doped Al-doped ZnO (AZO:Ag) increased to 10.20% of PCE from 9.08% PCE of the reference PSCs with pure AZO layer, but show inferior stability. Furthermore, PSCs with FDA modified AZO:Ag layer obtained 10.0% of PCEs and showed superior UV durability and moisture stability. PSCs with FDA modified AZO:Ag layer respectively maintain the original PCE values of 50% and 53% exposing UV light for 13 h and aging for 9 months at RH 10%, which are obviously higher than 36% and 34% of the original PCEs of PSCs with AZO:Ag layer. The results indicate that FDA modification is an effective strategy to solve the quick deterioration of plasmonic PSCs without evidently sacrificing PCEs.

## 1. Introduction

In the past decades, polymer solar cells have been intensively studied due to their low-cost, flexibility, and ease for large area manufacturing on flexible substrates [1, 2]. In order to enhance the performance of PSCs, many approaches have been developed including fabricating the low gap polymer [3, 4], designing non-fullerene acceptors [5, 6], optimizing the film nanoscale morphology [7, 8], functional modification layer [9, 10] and introducing solvent additives [11, 12]. Recently, great achievements have been made for PSCs in past two years, with the PCE of bulk-heterojunction over 15% [13], which are gradually approaching to PCE of commercial application. However, further improving efficiency and stability of PSCs are still two main aims to realize the industrial application.

Metal nanostructures have been extensively incorporated into PSCs to boost the performance because of plasmon-optical effects [14, 15]. In general, the plasmonic resonances of nanomaterials are sorted as surface plasmonic resonance (SPR) of grating structures and localized surface plasmonic resonance (LSPR) of NPs [16]. LSPR is defined that the collective electron charge oscillation in metal NPs and discrete nanostructures is excited by light. LSPR effects are related to the size, shape, composition and the dielectric properties of their surroundings [15]. LSPR effects can effectively enhance light absorption of photo-active layer by incorporating metal NPs into hole transport layer (HTL), photo-active layer and electron transport layer (ETL), respectively [17–19]. Furthermore, metal NPs doped into the carrier transport layer can usually reduce the serial resistance and inhibit carrier recombination, and thus improve extraction and carrier transport abilities [20]. However, plasmonic PSCs incorporated with Ag or Au NPs can accelerate the performance deterioration due to the diffusion of Ag and Au atoms and the wriggle and accumulation of metal NPs [21, 22]. AgAl alloy NPs

incorporated plasmonic PSCs can obviously enhance the stability of cells, because the formed  $\text{AlO}_x$  at the surface of AgAl NPs can suppress the diffusion of Ag NPs and accumulation of AgAl nanostructures [20]. However, metal alloy NPs usually need more complicated fabrication condition, which would limit the flexibility of application. The pure Ag and Au NPs are easily synthesized using chemical method and can flexibly incorporate into different function layer of PSCs. Although plasmon-enhanced PSCs incorporating pure noble metals NPs have massively been reported, yet their stability has hardly been revealed [17, 18]. Therefore, investigating and improving the stability of plasmon-enhanced PSCs based on pure Ag and Au NPs is an important and challenge work to realize the industrial application of plasmonic PSCs.

Recently, Ferrocene derivatives has been concerned due to its superior reversibility, rapid reaction, chemical stability [23–25]. Ferrocenecarboxylic acid, which contained ferrocene group into molecular or supra-molecular structures is extensively used as molecular sensor and charge transfer catalyzer [26, 27]. It can be applied in coordination chemistry because of its outstanding performance such as superior redox activity, high thermal stability and facilitated enzymatic activity [28, 29]. FDA was firstly introduced into  $\text{NiO}_x$  as a HTL interfacial modified layer of perovskite solar cells, which improved the contact characteristics and reduced defects of the  $\text{NiO}_x$  layer [30]. Furthermore, perovskite solar cells with FDA modified  $\text{NiO}_x$  layer present superior UV stability and a hysteresis-free effect, indicating that the ferrocene derivatives have potential application to improve UV durability and PCEs of PSCs due to their many common properties between perovskite solar cells and polymer solar cells.

In this work, FDA and Ag NPs were together integrated into AZO electron transport layer to commonly improve PCEs and stability of PSCs. The stability of PSCs with FDA-modified AZO:Ag layer was significantly increased compared to cells with AZO:Ag layer, suggesting that FDA modification is an effective method to enhance the stability of plasmonic PSCs.

## 2. Experimental section

The indium tin oxide (ITO) deposited on glass substrates with sheet resistance of  $10 \Omega/\square$  were washed in sequence with detergent, deionized water, acetone and isopropyl alcohol by using ultrasonic wave cleaning each cleaning progress for 20 min, then blow dried with nitrogen gas and immersed in ultraviolet ozone for 20 min. The electron transfer layers with AZO, AZO:Ag, FDA modified AZO and FDA modified AZO:Ag were fabricated, respectively. According to the published literature [31], 4 mmol of Zinc acetate ( $\text{Zn}(\text{CH}_3\text{CO}_2)_2 \cdot 2\text{H}_2\text{O}$ ) and 0.02 mmol of aluminum nitrate ( $\text{Al}(\text{NO}_3)_3 \cdot 9\text{H}_2\text{O}$ ) were mixed together in 10 ml of ethanol and stirred for 4 h at  $60^\circ\text{C}$ . AZO:Ag solution were prepared as follow: (1) firstly, mixed 0.1 mmol of  $\text{AgNO}_3$ , 25 ml of ethylene glycol and 0.5 g of PVP-10 together with stirred for 1 h at  $120^\circ\text{C}$ . (2) Then, the mixed solution was centrifuged several times and the sediments were dispersed into ethanol to obtain the silver colloid. (3) The optimized AZO:Ag solution was obtained by adding Ag colloid ( $0.13 \text{ mmol ml}^{-1}$ ) into sol-gel AZO solution ( $0.4 \text{ mmol ml}^{-1}$ ) with the molar ratio of 1:6, which is corresponding to the mass ratio of 0.36 wt%. The AZO with and without Ag NPs solutions were spin-coated onto ITO films with 4000 rpm and put in drying oven at  $150^\circ\text{C}$  for 30 min to form 20 nm AZO and AZO:Ag thin films, respectively. Then FDA solution was spin-coated onto AZO and AZO:Ag layer with 3000 rpm to form a modified layer. The molecular structure of FDA is shown in figure 1(a). FDA powders (purchased from Sinopharm Chemical Reagent), were dissolved in chlorobenzene with a concentration of  $0.1 \text{ mg ml}^{-1}$ , then stirred at room temperature for 24 h. Figures 1(b) and (c) display the molecular structures of PTB7-Th (purchased from 1-Material INC) and PC71BM (purchased from Solenne BV). PTB7-Th (5 mg) and PC71BM (7.5 mg) with a 1:1.5 weight ratio were added into 1 ml chlorobenzene/1, 8-diiodooctane (97:3, v/v) solvent and stirred at room temperature for 24 h. The PTB7-Th:PC71BM blended solution was deposited onto AZO surface at 1000 rpm for 13 s in nitrogen-filled glove box to form the active layer with 80 nm thickness. Then  $\text{MoO}_3$  of 7 nm thickness and AgAl film with 100 nm were deposited by thermal evaporation, respectively. A typical structure of PSCs with Glass/ITO/AZO:Ag/FDA/PTB7-Th:PC71BM/ $\text{MoO}_3$ /AgAl is shown in figure 1(d). The aperture area with a mask is  $0.09 \text{ cm}^2$ .

The surface morphologies of samples were investigated by field-emission scanning electron microscopy (SEM) with a model of Hitachi S-4800. The current density-voltage ( $J-V$ ) characteristics of cells were measured with a SourceMeter (Keithley 2440) together using a Newport solar simulator (AM 1.5 G illumination of  $100 \text{ mW cm}^{-2}$ ) calibrated with a standard silicon reference cell. The incident-photon-to-current conversion efficiencies (IPCEs) of cells were measured with a Newport Optical Power Meter 2936-Rover. The dark current density-voltage characteristics of cells were measured using a Autolab PGSTAT 302 N electrochemical workstation. The absorption spectra of samples were recorded by a Hitachi U-3900 UV/vis spectrophotometer.

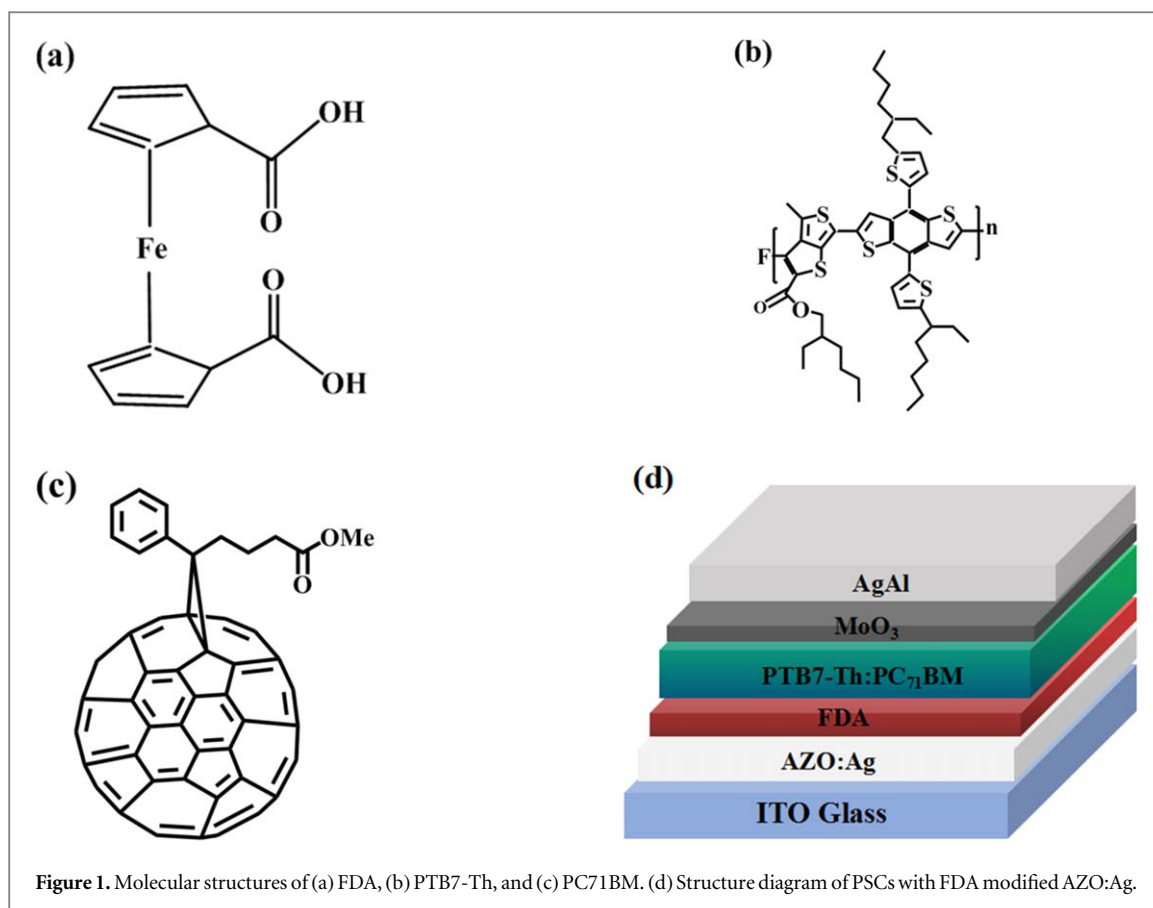
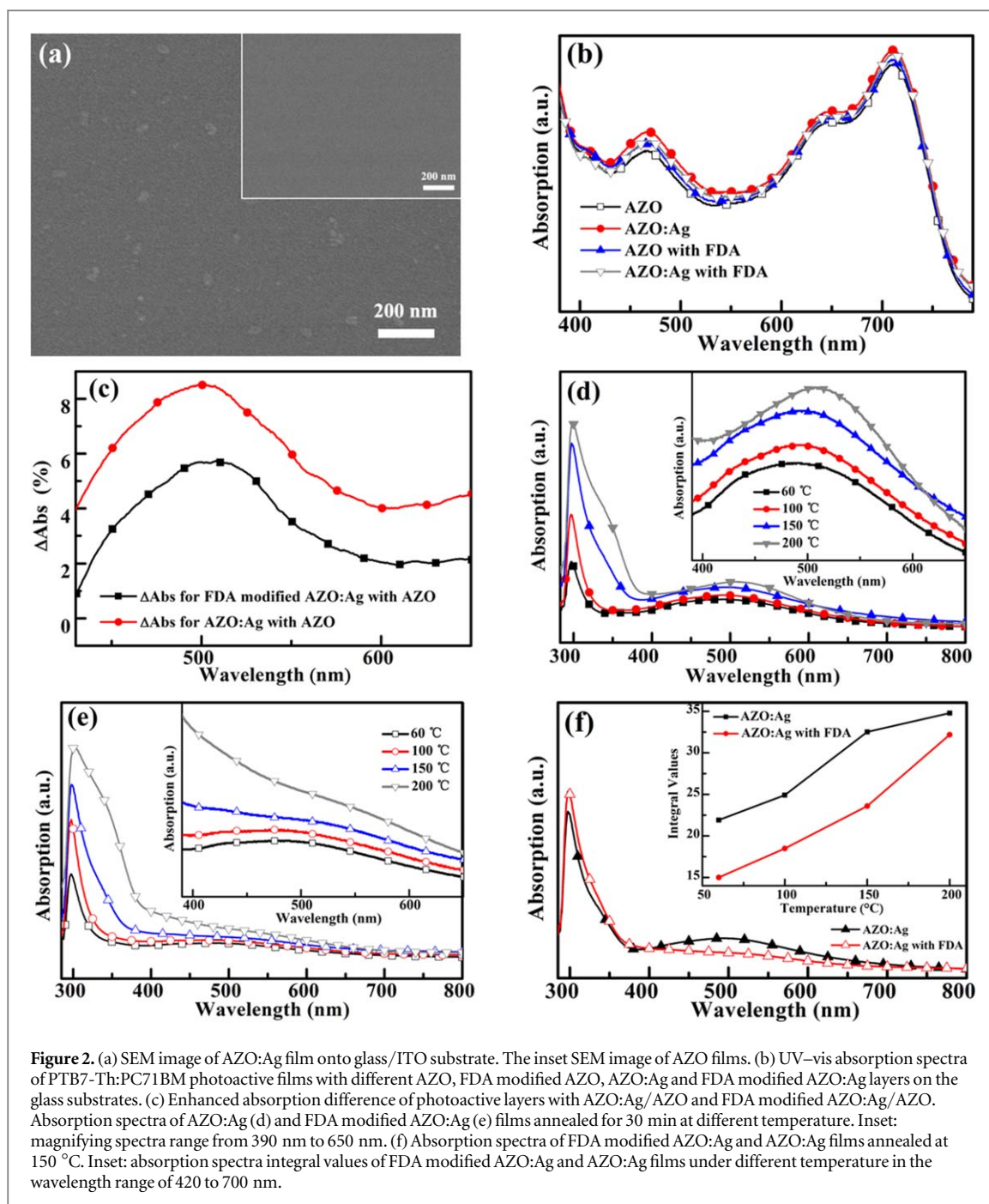


Figure 1. Molecular structures of (a) FDA, (b) PTB7-Th, and (c) PC71BM. (d) Structure diagram of PSCs with FDA modified AZO:Ag.

### 3. Results and discussion

The surface morphologies of AZO:Ag and AZO films are shown in figure 2(a). The film of AZO is very uniform without impurities. The white island-shaped nanostructures observed in AZO:Ag composite surface are Ag NPs islands due to its high conductivity. The absorption spectra of PTB7-Th:PC71BM films with different electron transport layers are shown in figure 2(b). The enhanced absorption difference of photoactive layers with AZO:Ag and FDA modified AZO:Ag compared to pure AZO at the wavelength range of 400 nm to 650 nm are shown in figure 2(c). The maximum absorption enhancement of photoactive layers with AZO:Ag and FDA modified AZO:Ag are respectively 8.5% and 5.7% due to LSPR effects. The relative weak absorption enhancement of PTB7-Th:PC71BM film onto FDA modified AZO:Ag compared to AZO:Ag, indicates that FDA modified Ag NPs can weaken LSPR effect of Ag NPs due to their coordinated interaction [18, 25]. Figures 2(d) and (e) show absorption spectra of AZO:Ag and FDA modified AZO:Ag with different annealing temperature, respectively. The gradually enhanced absorption intensities with increasing annealing temperature indicate that the shape, accumulation and surroundings changes of Ag NPs [15, 18]. In the meantime, the lower absorption intensity of FDA modified AZO:Ag compared to AZO:Ag films annealed at 150 °C in the wavelength range between 400 nm to 700 nm, as shown in figure 2(f), is consistent with the observed result of the lower absorption enhancement of PTB7-Th:PC71BM film onto FDA modified AZO:Ag, which further support the presumption that FDA modified Ag NPs can weaken LSPR effect. The absorption integral values between 420 nm and 700 nm of FDA modified AZO:Ag and AZO:Ag films with different temperature are shown in the inset of figure 2(f). Although the integral values of FDA modified AZO:Ag is obviously lower than that of AZO:Ag, the similar linear increasing trend is observed when annealing temperature increase from 60 °C to 150 °C. However, FDA modified AZO:Ag film shows quickly increasing trend with further increasing to 200 °C, which is possibly attributed to the reduced coordinated interaction between FDA and Ag atoms and improve the LSPR effects [25].

To investigate the integrated effects of plasmonic Ag NPs incorporation and FDA modification in the AZO layer on the performance of PSCs, four different cells were fabricated, respectively. The detailed parameters and the structure of these cells are shown in table 1. Typical  $J-V$  curves of cells with four different ETLs are shown in figure 3. PSCs with a AZO:Ag layer achieved a PCE = 10.2% with a  $J_{sc}$  = 19.5 mA cm<sup>-2</sup>,  $V_{oc}$  = 792 mV, FF = 66.1%, which is 13.4% higher than the PCE of the PSCs (9.08%) with pure AZO film. The higher  $J_{sc}$  and FF contribute to the enhanced PCEs of PSCs with AZO:Ag layer, which is primarily ascribed to LSPR effects and



**Figure 2.** (a) SEM image of AZO:Ag film onto glass/ITO substrate. The inset SEM image of AZO films. (b) UV-vis absorption spectra of PTB7-Th:PC71BM photoactive films with different AZO, FDA modified AZO, AZO:Ag and FDA modified AZO:Ag layers on the glass substrates. (c) Enhanced absorption difference of photoactive layers with AZO:Ag/AZO and FDA modified AZO:Ag/AZO. Absorption spectra of AZO:Ag (d) and FDA modified AZO:Ag (e) films annealed for 30 min at different temperature. Inset: magnifying spectra range from 390 nm to 650 nm. (f) Absorption spectra of FDA modified AZO:Ag and AZO:Ag films annealed at 150 °C. Inset: absorption spectra integral values of FDA modified AZO:Ag and AZO:Ag films under different temperature in the wavelength range of 420 to 700 nm.

**Table 1.** Performance of PSCs with structure of ITO/ETLs/PTB7-Th:PC71BM/MoO<sub>3</sub>/AgAl.  $R_s$  is derived from  $J-V$  curves at  $V_{oc}$ .

ETLs	$V_{oc}$ (mV)	$J_{sc}$ (mA cm <sup>-2</sup> )	FF (%)	PCE (%)	$R_s$ ( $\Omega$ .cm <sup>2</sup> )
AZO	785 ± 3	17.7 ± 0.3	64.5 ± 1.3	8.97 ± 0.20	42.3
AZO:Ag	793 ± 3	19.1 ± 0.4	66.1 ± 1.1	9.99 ± 0.30	31.2
AZO with FDA	785 ± 3	18.6 ± 0.4	64.8 ± 1.4	9.47 ± 0.30	36.4
AZO:Ag with FDA	789 ± 3	19.0 ± 0.3	65.5 ± 1.2	9.85 ± 0.20	31.6

reduced resistance due to Ag NPs incorporation [20]. PSCs with FDA modified AZO layer achieve a PCE = 9.66% with a  $J_{sc}$  = 19.0 mA cm<sup>-2</sup>,  $V_{oc}$  = 790 mV, FF = 64.3%, which is 6.3% higher than the PCE of PSCs (9.08%) with pure AZO film. The improved PCE of cells with FDA modified AZO is primarily due to excellent conductivity and outstanding contact properties [30]. PSCs based on FDA modified AZO:Ag layer exhibit an  $V_{oc}$  of 792 mV, a  $J_{sc}$  of 19.3 mA cm<sup>-2</sup>, a FF of 65.4% with a corresponding PCE of 10.0%, which is

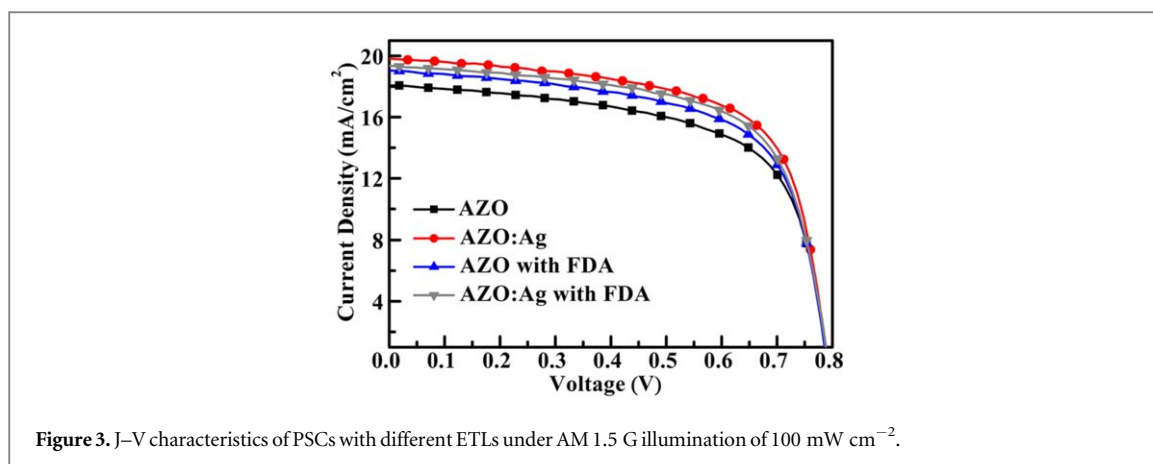


Figure 3. J–V characteristics of PSCs with different ETLs under AM 1.5 G illumination of  $100 \text{ mW cm}^{-2}$ .

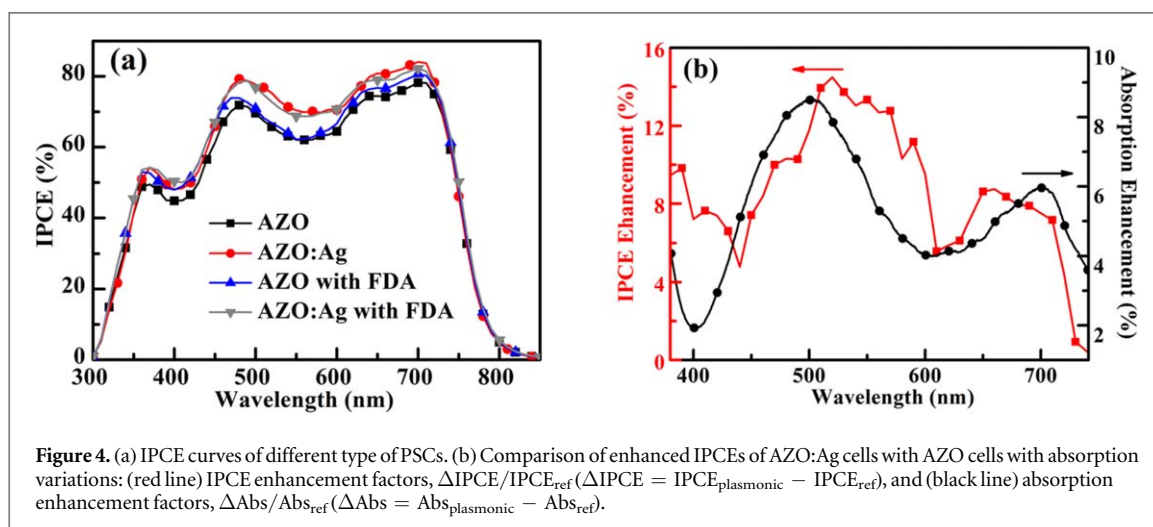


Figure 4. (a) IPCE curves of different type of PSCs. (b) Comparison of enhanced IPCEs of AZO:Ag cells with AZO cells with absorption variations: (red line) IPCE enhancement factors,  $\Delta\text{IPCE}/\text{IPCE}_{\text{ref}}$  ( $\Delta\text{IPCE} = \text{IPCE}_{\text{plasmonic}} - \text{IPCE}_{\text{ref}}$ ), and (black line) absorption enhancement factors,  $\Delta\text{Abs}/\text{Abs}_{\text{ref}}$  ( $\Delta\text{Abs} = \text{Abs}_{\text{plasmonic}} - \text{Abs}_{\text{ref}}$ ).

obviously higher than PCEs of cells with AZO and FDA modified AZO layers. The average PCE of PSCs with FDA modified AZO:Ag is 9.85%, which is slightly lower than average PCE (9.99%) of PSCs with AZO:Ag layer, indicating that FDA modified Ag NPs can slightly limit the function of plasmon-enhanced PSCs with AZO:Ag layer.

In order to investigate the reason of the improved  $J_{\text{sc}}$  of plasmonic PSCs, the IPCE curves of different PSCs are shown in figure 4(a). The IPCE of PSCs with AZO:Ag layer is clearly higher than that of cells with pure AZO layer in the wavelength region of 350–720 nm. The difference of IPCE values between PSCs with AZO:Ag and pure AZO is shown in figure 4(b). The enhanced  $\Delta\text{IPCE}$  curve roughly matches with the improved absorption spectra profiles of PTB7-Th:PC<sub>71</sub>BM onto the AZO:Ag films, indicating that LSPR effects of Ag NPs help to enhance IPCE values. However, the average values of the  $\Delta\text{Abs}$  obtained from the absorption spectra is lower than the  $\Delta\text{IPCE}$ , indicating the improved IPCE is partly attributed to the LSPR of Ag NPs. The reduced serial resistance and improved contact properties can also contribute to PCEs of plasmonic PSCs [22].

To further confirm the reasons of the  $J_{\text{sc}}$  enhancement, the maximum exciton generation rates ( $G_{\text{max}}$ ) and photocurrent density ( $J_{\text{ph}}$ ) against the effective voltage ( $V_{\text{eff}}$ ) were determined [20]. Figure 5 presents plots of  $J_{\text{ph}}$  versus  $V_{\text{eff}}$  for the devices with four different ETLs. Here,  $J_{\text{ph}}$  can be defined as  $J_{\text{ph}} = J_{\text{l}} - J_{\text{d}}$ , where  $J_{\text{l}}$  and  $J_{\text{d}}$  are the current densities under light and in the dark, respectively.  $V_{\text{eff}}$  is determined as  $V_{\text{eff}} = V_0 - V_{\text{a}}$ , where  $V_0$  is the voltage when  $J_{\text{ph}} = 0$  and  $V_{\text{a}}$  is the applied bias voltage.  $J_{\text{ph}}$  was found to increase linearly with  $V_{\text{eff}}$  in the low- $V_{\text{eff}}$  range and tend to saturate gradually at high  $V_{\text{eff}}$ . The saturated  $J_{\text{ph}}$  at large reverse bias is the saturation current density ( $J_{\text{sat}}$ ), which is primarily limited by the total amount of absorbed incident photons [20]. Additionally,  $G_{\text{max}}$  can be calculated using the equation  $J_{\text{sat}} = qG_{\text{max}}L$ , where  $q$  is the electronic charge and  $L$  is the thickness of the active layer with 80 nm. From figure 5,  $G_{\text{max}}$  values of PSCs can be determined as  $1.48 \times 10^{28} \text{ m}^{-3} \cdot \text{s}^{-1}$  ( $J_{\text{sat}} = 189 \text{ A m}^{-2}$ ),  $1.72 \times 10^{28} \text{ m}^{-3} \cdot \text{s}^{-1}$  ( $J_{\text{sat}} = 220 \text{ A m}^{-2}$ ),  $1.61 \times 10^{28} \text{ m}^{-3} \cdot \text{s}^{-1}$  ( $J_{\text{sat}} = 206 \text{ A m}^{-2}$ ) and  $1.71 \times 10^{28} \text{ m}^{-3} \cdot \text{s}^{-1}$  ( $J_{\text{sat}} = 219 \text{ A m}^{-2}$ ) for cells with structure of AZO, AZO:Ag, FDA-modified AZO and FDA-modified AZO:Ag layers, respectively. The noticeable enhancements in  $J_{\text{sat}}$  and  $G_{\text{max}}$  support optical absorption enhancement of the photoactive layer for cells with FDA modified AZO and FDA modified AZO:Ag [20]. The  $[P(E, T)]$  is defined as  $J_{\text{ph}}/J_{\text{sat}}$ , which means carrier transport and collection probabilities [22]. The

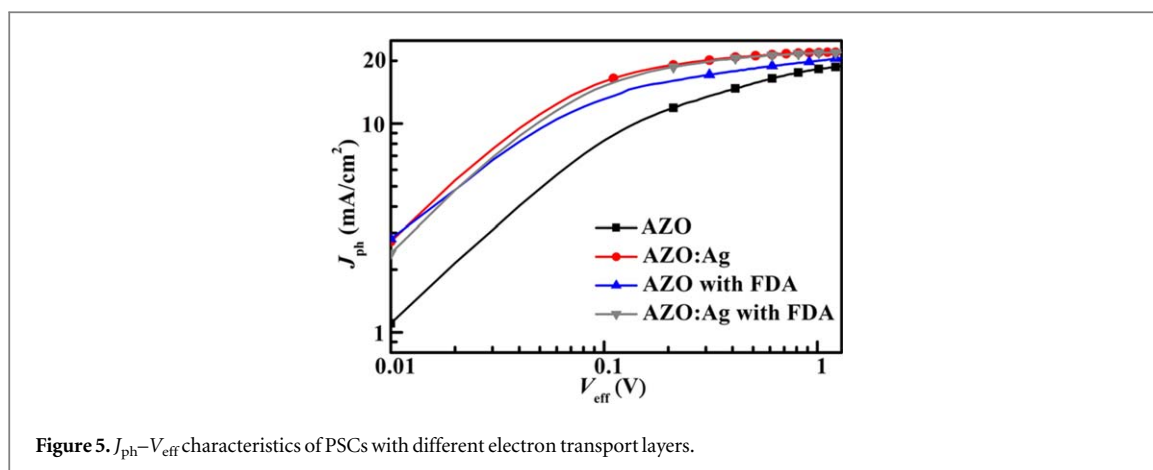
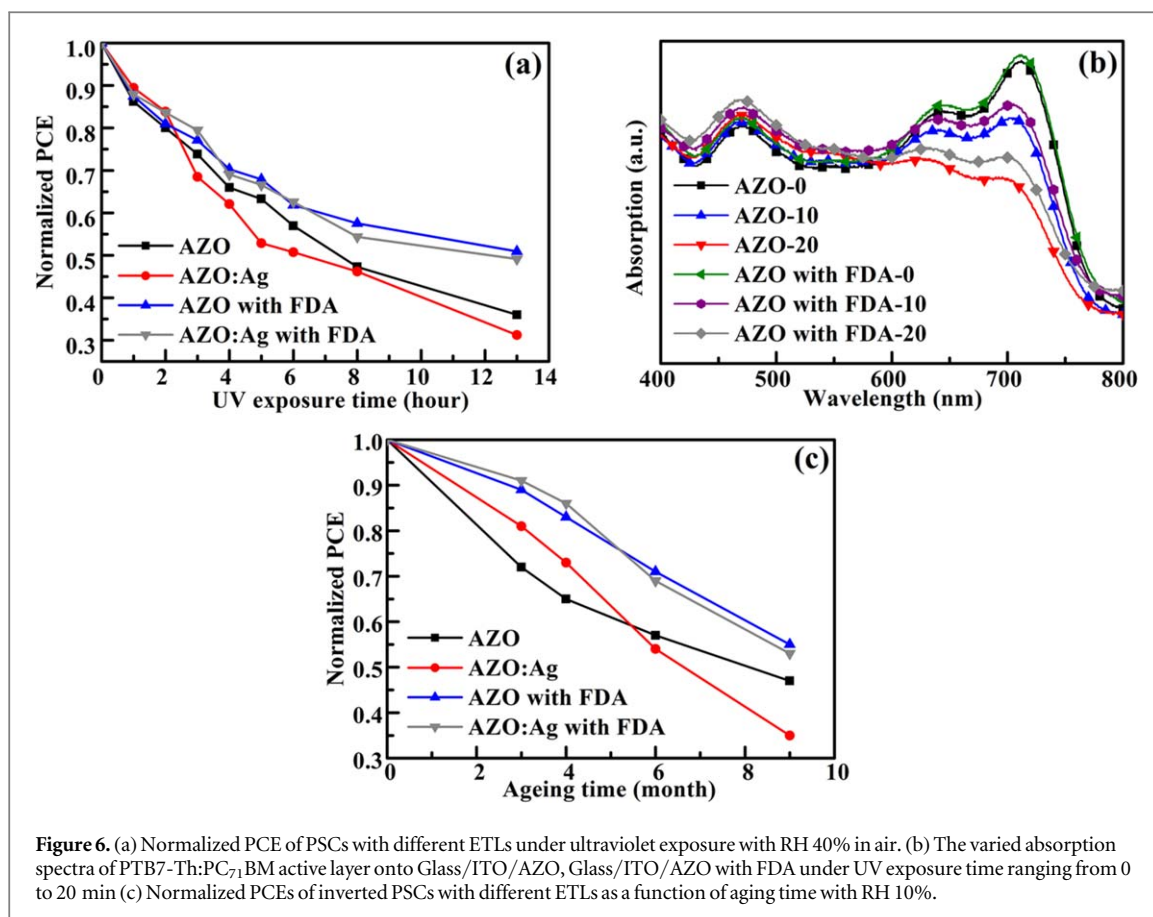


Figure 5.  $J_{ph}$ - $V_{eff}$  characteristics of PSCs with different electron transport layers.

values of P(E, T) for PSCs with AZO, FDA modified AZO, AZO:Ag and FDA modified AZO:Ag are 87.2%, 90.3%, 93.4% and 93.6%, respectively. The P(E, T) of cells with FDA modified AZO is obviously increased to 90.3% than that (87.2%) of cells with pure AZO, indicating that FDA modification in AZO layer can improve electron transport and collection probabilities. The P(E, T) value of cells with AZO:Ag is significantly higher than that of cells with pure AZO, suggesting that doping Ag NPs into AZO helps to improve electron transport and collection probabilities. However, FDA modified AZO:Ag compared to AZO:Ag layer cannot further improve its P(E, T) value, indicating that the strategy of doping Ag NPs into AZO layer has enough role to improve the contact property and increase the conductivity of electron transport layer, which is further supported from the similar  $R_s$  values and fill factor ( $FF$ ) of cells with FDA modified AZO:Ag and AZO:Ag, as shown in table 1 [32].

Plasmonic PSCs with pure Ag and Au NPs usually accelerate the deterioration, which would reduce the value of the practical application [20, 21]. The photoactive layer and interfacial layers can accelerate degradation under the exposure of UV, oxygen and moisture. The oxygen and moisture effects can be well overcome by the superior encapsulation technology [33]. However, the degradation induced by UV irradiation cannot be completely avoided even using UV filter method. UV irradiation can induce numerous deep trap states, which leading to charge recombination and more quickly degrade the active layer [30]. Therefore, UV durability is an special important parameter for polymer solar cells [34]. A UV-induced acceleration degradation of devices of four types of PSCs without encapsulation under an air environment with a relative humidity of (RH) of 40% was used to evaluate UV stability. Normalized PCE of PSCs with different ETLs under UV exposure with RH 40% are shown in figure 6(a). The cells with AZO:Ag and pure AZO were quickly decreased and respectively reached 30% and 36% of the original PCE values under UV exposure for 13 h, indicating that doping Ag NPs can promote the deterioration of cells, which is consistent with the previous reported results [20, 21]. However, the PCEs of PSCs with FDA modified AZO and FDA modified AZO:Ag keep similar UV stability and remain about 50% of the initial PCE value, indicating that FDA modification have obvious role to improve UV stability. The varied absorption spectra of the photoactive layer with AZO and FDA modified AZO substrates with different time of UV exposure are shown in figure 6(b). There are three obvious peaks located in 470 nm, 645 nm and 710 nm, respectively. The relative absorption of the peak in 710 nm was more quickly weaken and gradually blue-shifted to 703 nm with increasing UV exposure time, which is attributed to the broken of conjugated bonds of PTB7-Th polymer reducing the electron delocalized state [35]. However, the degradation of the PTB7-Th polymer onto FDA modified AZO:Ag layer can be obviously suppressed, which further support that FDA has function of improving UV stability of PSCs. Figure 6(c) shows PCEs of unencapsulated PSCs with different ETLs as a function of aging time under RH 10% condition. PSCs with FDA modified AZO:Ag and FDA modified AZO show similar degradation trend and were decreased to about 53% of the original PCEs ageing for 9 months, which are superior PCEs of PSCs with AZO:Ag (35%) and pure AZO layer (47%). These results indicate that FDA modification have dual functions to improve moisture and UV resistance of plasmonic PSCs.

Ag NPs doped into carrier transport layers have been demonstrated to obviously improve the PCEs of PSCs [21, 36, 37], the diffusion of Ag atoms can usually speed up the deterioration of cells during UV exposure, because the carrier transport layer would be produce more vacancies under the interaction of UV light [34]. Ferrocene derivatives can always interact with noble metal such as Au and Ag NPs, which can stabilize noble metal NPs [25, 38]. Although the deep mechanism of improving the stability of plasmonic PSCs would be further investigated in future, FDA modification is an effective strategy to solve the stability of plasmonic PSCs.



#### 4. Conclusions

The PCE of PSCs with FDA-modified AZO reached 9.66%, which is clearly higher than that of the cells with pure AZO (9.08%), suggesting that FDA modified electron transport layer is an efficient way to promote PCEs of PSCs. Cells with FDA modified AZO:Ag can further increase to PCE of 10.0% because of Ag NPs LSPR effects. PSCs with FDA modified AZO:Ag and AZO layers show similar UV and moisture stability, which are obviously superior that of PSCs with AZO:Ag and AZO layer, indicating that FDA modification is an effective strategy to solve the stability of plasmonic PSCs. Considering the common properties between perovskite solar cells and polymer solar cells, the similar strategy would be increased the stability of plasmonic perovskite solar cells.

#### Acknowledgments

This work was supported by Natural Science Foundation of Shanghai (Nos. 18ZR1411000 and 18ZR1411900).

#### ORCID iDs

Sumei Huang <https://orcid.org/0000-0001-5283-3918>

Wei Ou-Yang <https://orcid.org/0000-0002-0511-9225>

Xiaohong Chen <https://orcid.org/0000-0002-4441-346X>

#### References

- [1] Choi S, Zhou Y, Haske W, Shim J W, Fuentes-Hernandez C and Kippelen B 2015 ITO-free large-area flexible organic solar cells with an embedded metal grid *Org. Electron.* **17** 349–54
- [2] Yao H, Ye L, Zhang H, Li S, Zhang S and Hou J 2016 Molecular design of benzodithiophene-based organic photovoltaic materials *Chem. Rev.* **116** 7397–457
- [3] Yao H, Chen Y, Qin Y, Yu R, Cui Y, Yang B, Li S, Zhang K and Hou J 2016 Design and synthesis of a low bandgap small molecule acceptor for efficient polymer solar cells *Adv. Mater.* **28** 8283–7
- [4] Yang Y et al 2018 High-efficiency organic solar cells based on small-molecule donor and low-bandgap polymer acceptor with strong absorption *J. Mater. Chem. A* **6** 9613–22

- [5] Liu Z, Wu Y, Zhang Q and Gao X 2016 Non-fullerene small molecule acceptors based on perylene diimides *J. Mater. Chem. A* **4** 17604–22
- [6] Cheng P, Li G, Zhan X and Yang Y 2018 Next-generation organic photovoltaics based on non-fullerene acceptors *Nat. Photon.* **12** 131–42
- [7] Yang X, Loos J, Veenstra S C, Verhees W J H, Wienk M M, Kroon J M, Michels M A J and Janssen R A J 2005 Nanoscale morphology of high-performance polymer solar cells *Nano Lett.* **5** 579–83
- [8] Kumar A, Li G, Hong Z and Yang Y 2009 High efficiency polymer solar cells with vertically modulated nanoscale morphology *Nanotechnology* **20** 65202 (4pp)
- [9] Wang Y, Tong S W, Xu X F, Özyilmaz B and Loh K P 2011 Interface engineering of layer-by-layer stacked graphene anodes for high-performance organic solar cells *Adv. Mater.* **23** 1514–8
- [10] Seo J H, Gutacker A, Sun Y, Wu H, Huang F, Cao Y, Scherf U, Heeger A J and Bazan G C 2011 Improved high-efficiency organic solar cells via incorporation of a conjugated polyelectrolyte interlayer *J. Am. Chem. Soc.* **133** 8416–9
- [11] Sun Y, Welch G C, Leong W L, Takacs C J, Bazan G C and Heeger A J 2012 Solution-processed small-molecule solar cells with 6.7% efficiency *Nat. Mater.* **11** 44–8
- [12] Zhao J, Li Y, Yang G, Jiang K, Lin H, Ade H, Ma W and Yan H 2016 Efficient organic solar cells processed from hydrocarbon solvents *Nature Energy* **1** 1–7
- [13] Yuan J et al 2019 Single-junction organic solar cell with over 15% efficiency using fused-ring acceptor with electron-deficient core *Joule* **3** 1–12
- [14] Yao M, Jia X, Liu Y, Guo W, Shen L and Ruan S 2015 Surface plasmon resonance enhanced polymer solar cells by thermally evaporating Au into buffer layer *Appl. Mater. Interfaces* **7** 18866–71
- [15] Huntter E and Fendler J H 2004 Exploitation of localized surface plasmon resonance *Adv. Mater.* **16** 1685–706
- [16] Mayer K M and Hafner J H 2011 Localized surface plasmon resonance sensors *Chem. Rev.* **111** 3828–57
- [17] Gan Q, Bartoli F J and Kafafi Z H 2013 Plasmonic-Enhanced organic photovoltaics: breaking the 10% efficiency barrier *Adv. Mater.* **25** 2385–96
- [18] Srivastava A, Samajdar D P and Sharma D 2018 Plasmonic effect of different nanoarchitectures in the efficiency enhancement of polymer based solar cells: a review *Sol. Energy* **173** 905–19
- [19] Chen X, Zhao C, Rothberg L and Ng M 2008 Plasmon enhancement of bulk heterojunction organic photovoltaic devices by electrode modification *Appl. Phys. Lett.* **93** 123302
- [20] Wang J, Jia X, Zhou J, Pan L, Huang S and Chen X 2016 Improved performance of polymer solar cells by thermal evaporation of AgAl alloy nanostructures into the hole-transport layer *Appl. Mater. Interfaces* **8** 26098–104
- [21] Lu Z, Chen X, Zhou J, Jiang Z, Huang S, Zhu F, Piao X and Sun Z 2015 Performance enhancement in inverted polymer solar cells incorporating ultrathin Au and LiF modified ZnO electron transporting interlayer *Organ. Electron.* **17** 364–70
- [22] Jia X, Jiang Z, Chen X, Zhou J, Pan L, Zhu F, Sun Z and Huang S 2016 Highly efficient and air stable inverted polymer solar cells using LiF-modified ITO cathode and MoO<sub>3</sub>/AgAl alloy Anode *Appl. Mater. Interfaces* **8** 3792–9
- [23] Dai L X, Tu T, You S L, Deng W P and Hou X L 2003 Asymmetric catalysis with chiral ferrocene ligands *Acc. Chem. Res.* **36** 659–67
- [24] Raoof J B, Ojani R and Kolbadinezhad M 2005 Electrocatalytic characteristics of ferrocenecarboxylic acid modified carbon paste electrode in the oxidation and determination of L-cysteine *Electroanalysis* **17** 2043–51
- [25] Astruc D 2017 Why is ferrocene so exceptional *Eur. J. Inorg. Chem.* **2017** 6–29
- [26] Ojani R, Raoof J B and Alinezhad A 2002 Catalytic oxidation of sulfite by ferrocenemonocarboxylic acid at the glassy carbon electrode. Application to the catalytic determination of sulfite in real sample *Electroanalysis* **14** 1197–202
- [27] Carollo L, Curulli A and Floris B 2003 Arylferrocenylmethanols: a new family of ferrocenes to be used as mediators in biosensors *Appl. Organomet. Chem.* **17** 589–99
- [28] Zhu C C, Yang L G, Li D C, Zhang Q F, Dou J M and Wang D Q 2011 Synthesis, characterization, crystal structure and antitumor activity of organotin(IV) compounds bearing ferrocenecarboxylic acid *Inorg. Chim. Acta* **375** 150–7
- [29] Ndamaniha J C and Guo L P 2008 Electrochemical determination of uric acid at ordered mesoporous carbon functionalized with ferrocenecarboxylic acid-modified electrode *Biosens. Bioelectron.* **23** 1680–5
- [30] Zhang J, Luo H, Xie W, Lin X, Hou X, Zhou J, Huang S, Ou-Yang W, Sun Z and Chen X 2018 Efficient and ultraviolet durable planar perovskite solar cells via a ferrocenecarboxylic acid modified nickel oxide hole transport layer *Nanoscale* **10** 5617–25
- [31] Jia X, Zhou J, Huang S, Ou-Yang W, Sun Z and Chen X 2017 Improved longtime stability of highly efficient polymer solar cells by accurately self-formed metal oxide interlayer at metal electrode *Sol. Energy* **157** 811–7
- [32] Choy W C H and Ren X 2016 Plasmon-electrical effects on organic solar cells by incorporation of metal nanostructures *IEEE J. Sel. Top. Quantum Electron.* **22** 1–9
- [33] Weerasinghe H C, Dkhissi Y, Scully A D, Caruso R A and Cheng Y 2015 Encapsulation for improving the lifetime of flexible perovskite solar cells *Nano Energy* **18** 118–25
- [34] Lin X, Luo H, Jia X, Wang J, Zhou J, Jiang Z, Pan L, Huang S and Chen X 2016 Efficient and ultraviolet durable inverted polymer solar cells using thermal stable GZO-AgTi-GZO multilayers as a transparent electrode *Org. Electron.* **39** 177–83
- [35] Chen X, Wang Z, Hou Y, Xu Z and Xu X 2000 Photoluminescence quenching in poly(p-phenylene vinylene) derivatives *Displays* **21** 55–60
- [36] Kalfagiannis N, Karagiannidis P G, Pitsalidis C, Panagiotopoulos N T, Gravalidis C, Kassavetis S, Patsalas P and Logothetidis S 2012 Plasmonic silver nanoparticles for improved organic solar cells *Sol. Enger. Mat. Sol. C* **104** 165–74
- [37] Baek S, Park G, Noh J, Cho C, Lee C, Seo M, Song H and Lee J 2014 Au@Ag core-shell nanocubes for efficient plasmonic light scattering effect in low bandgap organic solar cells *ACS Nano* **8** 3302–12
- [38] Ciganda R, Irigoyen J, Gregurec D, Hernandez R, Moya S, Wang C, Ruiz J and Astruc D 2016 Liquid-liquid interfacial electron transfer from ferrocene to gold(III): an ultrasimple and ultrafast gold nanoparticle synthesis in water under ambient conditions *Inorg. Chem.* **55** 6361–3